Hindawi
Journal of Advanced Transportation
Volume 2022, Article ID 8830276, 9 pages
https://doi.org/10.1155/2022/8830276

Research Article

Innovative Smart Road Stud Sensor Network Development for Real-Time Traffic Monitoring

Zhimin Tao,[1] **Wei Quan**,[2] **and Hua Wang**[2]

[1]*School of Transportation Science and Engineering, Beihang University, Beijing, China*
[2]*School of Transportation and Science Engineering, Harbin Institute of Technology, Harbin, China*

Correspondence should be addressed to Hua Wang; huawang@hit.edu.cn

Received 27 May 2020; Accepted 21 February 2022; Published 5 May 2022

Academic Editor: Tom Hao Luan

Intelligent transportation infrastructure has gained significant research attention recently. In this paper, an innovative sensor network of smart road stud (SRS) is developed to enhance traffic detection infrastructure characterized by its functionality in traffic data collection, long/short range wireless data transmission, self-sustained power supply, and remote custom controlled lighting-based traffic guidance. Compared to the traditional traffic detectors and road studs, SRS nodes are installed on lane lines instead of lane center to enable the additional applications besides the detection function, such as traffic monitoring, congestion warning, routing guidance, and so on. SRS detects vehicles based on three-axis geomagnetic sensors. A vehicle detection algorithm is proposed correspondingly under different operation scenarios to count vehicles in two adjacent lanes. Its detecting accuracy can be further improved by a sensor network of multiple SRSs working cooperatively. Field test results show that the vehicle detection accuracy based on the SRS network is about 98% per lane, which is the same level as the commercial detector installed in center of lane, even under the non-standard driving behaviors such as crossing lane line. The high performance, value-added service, and low cost enable wide-range applications of SRS networks as part of intelligent traffic detection infrastructure.

1. Introduction

1.1. Background. Accurate traffic information collection is the premise to establish an intelligent transportation system and the basis to facilitate urban traffic operation plans, mitigate traffic congestion, and improve traffic safety. Monitoring technologies can be classified as intrusive, non-intrusive, and off-roadway. At present, typical traffic monitoring sensors on roadway mainly include inductive loop, geomagnetic detector, microwave radar, and video camera [1–4]. Inductive loop is the most accurate and stable traffic sensor which is the most widely used detector, but its relatively big size and the intrusive installation damage pavement surfaces and induce challenges in maintenance. Video camera and microwave radar are popular non-intrusive technologies. These sensors can be installed on roadsides without destroying pavement surfaces, but they are highly power-consuming and expensive. Lighting and weather conditions can affect their accuracy to generate a large amount of errors when there are vehicle occlusions. Geomagnetic sensor has unique advantages for its detection accuracy which is robust to weather conditions. It has small sizes and low costs and is easy to lay out as well as suitable for wireless communications [5–8].

Recently, GNSS data processing has becoming a very popular approach for traffic monitoring as an off-roadway technology because of its prevalence in personal devices and the applications beyond detection such as monitoring, vehicle tracking, and self-localization [9, 10]. However, the types of monitoring information provided are mainly aggregates (e.g., average speed and travel time) whose accuracy and timeliness mainly depend on vehicle probe density and the driving environment, which is not suitable for accurate monitoring of traffic flow rate and headway at the lane or road level.

The new traffic detection technology with high spatial resolution and high real-time performance has strong attraction and development potential, which can meet the

needs of precise location and assessment of traffic anomalies, driving safety assistance, traffic control, etc. However, the typical traffic detection technology is not suitable for high-density and distributed deployment due to the limitations of installation mode, cost, and maintenance, which are only installed in key points of roads [11]. This presents the following challenges for new detection techniques. (1) Sensor node are expected to have the characteristics of low power consumption, self-power supply, and long life. Wired power supply greatly increases the cost of hardware, installation, operation and maintenance, and greatly limits the high-density and distributed deployment requirements of smart devices. Fully self-powered road sensing nodes can greatly reduce the difficulty of sensing network deployment and improve system elasticity. (2) A linear distribution, stable, and reliable communication network is expected. (3) It is expected to achieve low-cost, multiservice function system to balance the economic benefits of large-scale deployment requirements. If large-scale deployment is to be realized, only the detection function lacks the attraction of engineering implementation. By integrating multi-service functions such as traffic safety assistance and navigation, the technology attraction is improved.

1.2. Smart Road Stud Sensing System. Road studs have been used widely for more than 75 years in many countries to delineate road lanes at night and in poor visibility. In this paper, the smart road stud (SRS) based on the geomagnetic principles is proposed to collect the geomagnetic disturbance information of vehicles in real time. The collected traffic data can be sent to the server by its wireless transmission module. In addition, solar panels can provide continuous power, and LED flash lighting functions can be highlight road lines and guide route selection and driving [12, 13]. SRS can be applied for vehicle detection, congestion monitoring, parking management, and driving guidance, and it demonstrates broad market prospects.

A traffic detection algorithm is investigated as well based on advanced hardware development. There are many ways to monitor traffic flow based on geomagnetic data. The dual-window detection method is widely used to extract vehicle waveform information [14–16], the finite state machine is also favored to detect vehicles [17–19], and the peak-to-trough method was developed based on adaptive thresholds to distinguish driving states of vehicles [20, 21]. In this paper, the vehicle driving state is judged based on the characteristics of the geomagnetic disturbance waveform caused by a vehicle passing an SRS. Through the cross section layout of SRS, the multi-channel data are integrated to realize the comprehensive detection of traffic flow. This method makes traffic detection more precise and comprehensive.

Compared to traditional vehicle detection methods, the SRS installed on the lane line can provide safety assurance by light guidance with the same correct detection rate as middle-installed intrusive sensor. The SRS system is actually part of smart infrastructure, whose surveillance function is one important basis for many relevant applications such as traffic/congestion monitoring, parking management, and so on. Its long-life cycle supports the potential to improve our understanding and ways to manage the safety, capacity, and overall efficiency of transportation networks. The versatility of the SRS makes it potentially scalable. Now, the SRS system has been used in confluence area route guidance and abnormal condition warning and other application scenarios.

The rest of the paper is structured as follows. Section 2 presents the SRS system architecture. Section 3 describes the preprocessing method for raw magnetic field data and the two-lane vehicle detection algorithm by a single SRS. Section 4 presents the vehicle detection algorithm by cooperative SRSs. Finally, the field test procedure is described and the results presented in Section 5. The paper is concluded in Section 6.

2. SRS Detection System

2.1. Installation Method. Geomagnetic detectors are commonly embedded in the center of lanes. Their detection accuracy could be affected by oversized vehicles passing in adjacent lanes or non-standard driving behavior such as vehicle crossing lanes [22].

Figure 1 indicates a typical working scenario of SRSs, which are installed on separation lane markings as traditional road studs to delineate road lanes, and the color can deliver different traffic information.

A SRS node consists of a microprocessor, a tri-axis geomagnetic sensor, a rechargeable battery/solar power module, a wireless transmission module, and a LED lighting module, which can support all the functions including vehicle detection, wireless data transmission, self-powering, and visual guidance. All the components are sealed in a protective case as a road stud of a diameter of 120 mm and a height of 35 mm. The tri-axis geomagnetic sensor is employed as the core component sufficient to detect the magnetic fields distorted by the passing vehicles. Compared with other traffic detection technologies, SRS is superior due to its compact, energy-efficient, low-cost, and multi-functional characteristics. Additionally, it is easy to install and maintain without damaging road surfaces. The functional structure of an SRS node and its appearance is shown in Figure 2.

In Figure 3, a 3-dimensional coordinate is established to show that the xx-axis of the geomagnetic sensor is the same as the driving direction, the yy-axis is perpendicular to the road direction, and the zz-axis is perpendicular to the road surface. B_{xx}, B_{yy}, and B_{zz} are the tri-axial magnetic induction values of an actual road surface sensor.

2.2. Geomagnetic Data Acquisition and Transmission. The SRS integrates two communication modes, which are Bluetooth 5.0 and Narrowband Internet of Things (NB-IoT), respectively, for local and remote communication. The collected data can be transmitted to the base station via NB-IoT and forwarded to its application server via the telecom platform. The NB-IoT multi-point uplink rate is 56 kbps, and the ideal downlink rate is 21.25 kbps. The

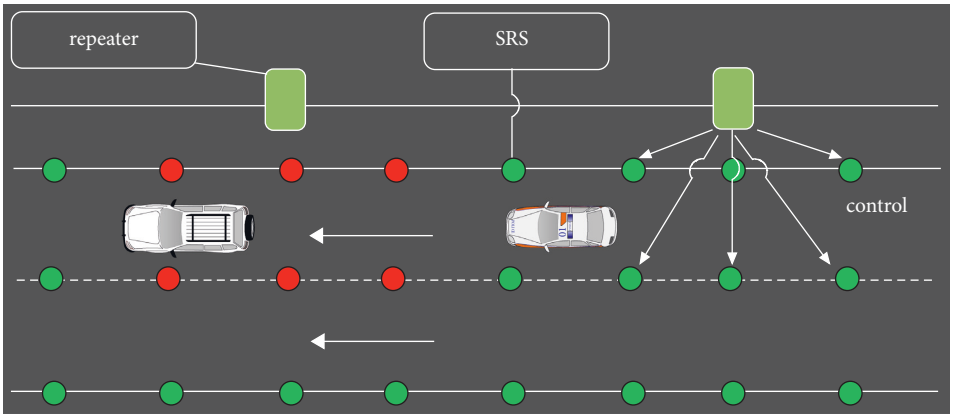

Figure 1: A typical working scenario of the SRS system.

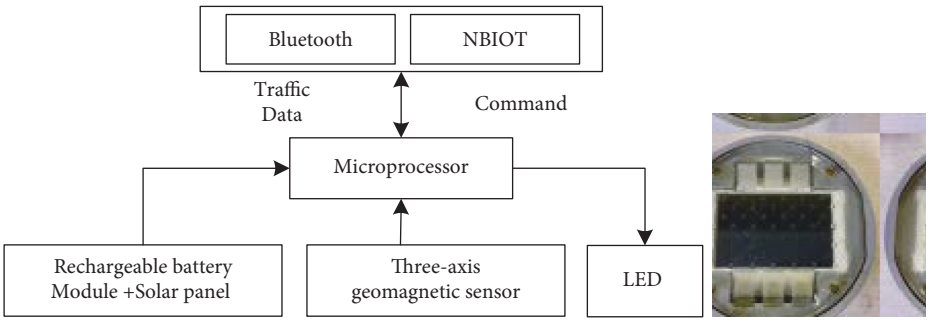

Figure 2: Physical and structural diagram of SRS.

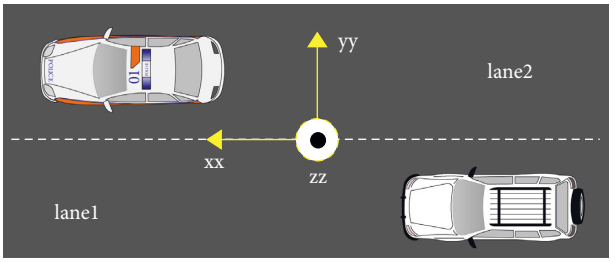

Figure 3: Orientation of the three-axis geomagnetic sensor.

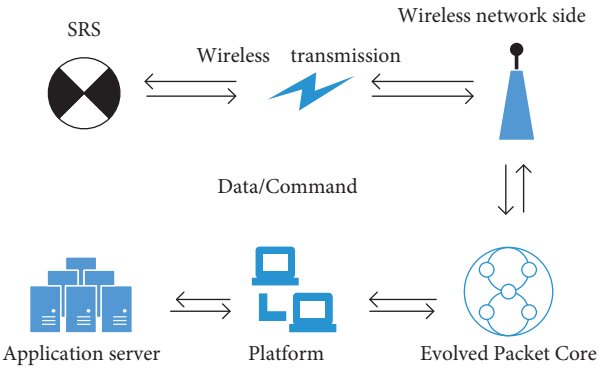

Figure 4: NB-IoT network topology.

sampling frequency used in the geomagnetic field is 100 HZ. By removing the invalid high-order data, a set of three-axis geomagnetic data can be 6 bytes, so the geomagnetic data rate is 600 bytes/s. A stud used in this study consumes about 60 mA on average when transmitting data using NB-IoT. It is unlikely to collect traffic data throughout a day, and using remote commands to set whether to enable data acquisition and transmission can significantly save energy.

The NB-IoT module is integrated inside a stud to enable remote data transmission. NB-IoT has a gain of 20 dB over the existing network and can cover areas that cannot be covered by deep underground GSM networks. The number of NB-IoT base stations is large, and each cell can handle 50 K connections, which is a huge connection necessary for realizing the Internet of Everything. NB-IoT supports PSM low-power modes with low power consumption and is integrated with eDRX technologies. An NB-IoT communication module costs less than $5. The NB-IoT network topology is shown in Figure 4.

In addition, SRSs allow adding repeaters on the roadside to control Bluetooth devices for data collection and aggregation. The roadside routing node can be powered by the regular power module or solar power system to ensure the full-day data collection. The Bluetooth function in a stud can guarantee at least a data transmission rate of 29 Kb/s, and the transmission of geomagnetic data to the concentrator can be easily realized. In the concentrator, 4G wireless signals or a network cable is used to realize geomagnetic data transmission with a large amount of data per day.

Additionally, the Bluetooth function can complete the local networking interaction task between the adjacent SRSs.

SRS nodes are managed and controlled locally by repeaters based on bluetooth low power protocol.

3. Single-SRS Vehicle Detection Algorithm

Around the Earth is a magnetic field with a strength of about 0.5-0.6 Gauss, which varies from place to place with the different geomagnetic inclination and declination angles. Vehicles are ferrous objects which can be magnetized by the Earth and disturbed by even 10% of the geomagnetic field. By detecting the magnetic field changes using the 3-axis geomagnetic sensor, the vehicle presence and operation conditions can be recognized.

3.1. Geomagnetic Data Acquisition. The geomagnetic data acquisition process is expressed as follows. After collecting raw geomagnetic data wirelessly by roadside units, an abnormal data process and a moving average smooth filtering algorithm are employed to reduce the signal noise in $B_{x,y,z}$. The geomagnetic data waveform is shown in Figure 5.

(1) Send acquisition commands which include start time and end time by the server.

(2) The command is transmitted to the stud via the NB-IoT module, and it returns a response confirmation message.

(3) Studs use internal RTC for data collection during specified periods.

(4) The data are cached inside the SRS until the packet reaches 512 bytes and then are transmitted to the server.

3.2. Vehicle Waveform Extraction. The dual window vehicle detection algorithm (DWVDA) is commonly used to extract vehicle waveforms from the raw geomagnetic data. The environmental effect such as temperature, humidity, and so on will affect the device electrical characteristics, which lead to the drift of the basic value and the accompanying error result instability of DWVDA. In this study, a new differential double window vehicle detection algorithm (D-DWVDA) is proposed to extract vehicle waveforms [23], which avoids the use of background values. The working principle of D-DWVDA and flowchart are shown in Figure 6.

W_{in} and W_{out} are defined as the vehicle arrival and vehicle departure windows, respectively. W_{w} is the time width of W_{in} and W_{out}, which is set as 0.1 s, which is significantly shorter than the time headway of safe distance between two following vehicles at the road speed limit. The heights of W_{in} and W_{out} are set as *ThresIn* and *ThresOut*, which are the threshold values of vehicles approaching and departing. By adjusting W_w, *ThresIn* and *Thresout* parameters, D-DWVDA has better adaptability to vehicle waveform extraction for different speed roads. $\Delta B_{x,y,z}$ are the differential sequences of $B_{x,y,z}$. The advantages of D-DWVDA lie in the differential value $\Delta B_{x,y,z}$ which can be used to decompose the cumulative errors caused by the basic value floating.

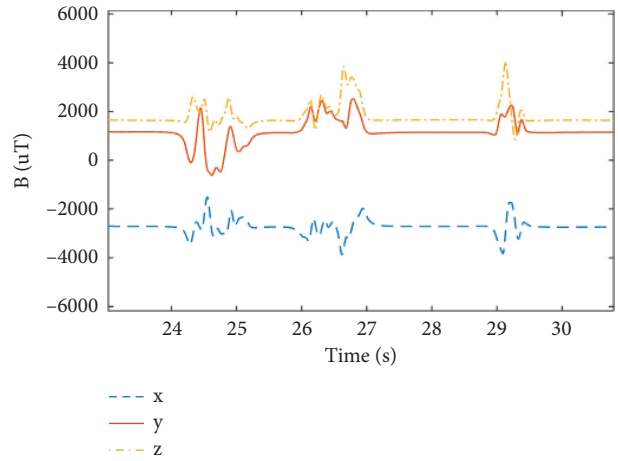

Figure 5: Raw geomagnetic data.

The working process is shown below.

(1) With no vehicle passing, all $\Delta B_{x,y,z}$ values are located in W_{in}.

(2) If all the points of any axis of $\Delta B_{x,y,z}$ exceed W_{in}, a vehicle is approaching and waveform extraction is started.

(3) When all the $\Delta B_{x,y,z}$ values are located in W_{out}, the vehicle is departing, and waveform extraction is terminated.

3.3. Two-Lane Vehicle Detection by a Single SRS. For two-lane vehicle detection, there are typically five working scenarios as shown in Figure 7.

Scenario 1: a vehicle passes by the left lane of an SRS, which is recorded as S (1,0).

Scenario 2: a vehicle passes by the right lane of an SRS, which is recorded as S (0,1).

Scenario 3: a vehicle passes over an SRS, which is recorded as S (1,1).

Scenario 4: two vehicles pass through an SRS in parallel, which is recorded as S (1,1).

Scenario 5: vehicle tire occupies lane makings, which is recorded as S (1,1) (Scenario 5 can be merged with Scenario 3 because their waveforms are similar).

The eigenvalues selected to distinguish the vehicle positions are $\{num_p, num_t, B_{\max}, B_{\min}, T, T_p/T, T_t/T\}$, which, respectively, represent the peak number, the trough number, the waveform maximum value, the minimum value, the waveform duration, the maximum value, and the relative position of maximum and minimum. Figure 8 shows a waveform corresponding to the five scenarios in Figure 7. The single SRS has a poor ability to identify the magnetic field of complex driving status in Scenarios 3, 4, and 5, which is the main error source of the detection. By data fusion and crossing validation among individual SRS, the discrimination of Scenarios 3, 4, and 5 can be accomplished to achieve high detection accuracy of each lane,

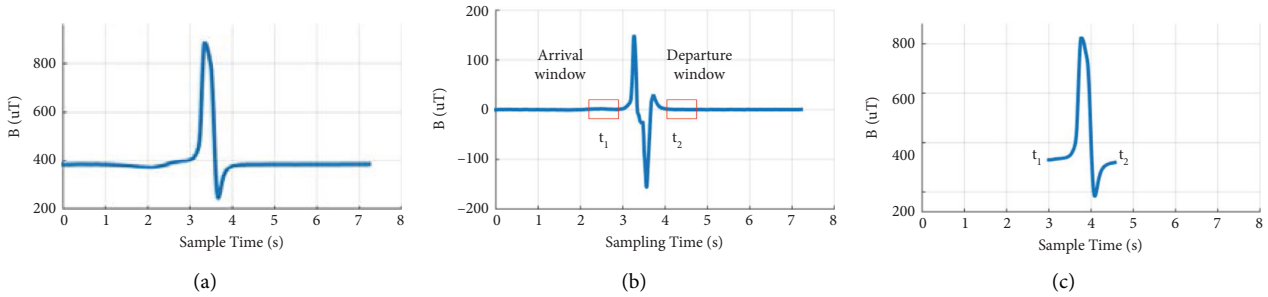

Figure 6: General view of D-DWVDA. (a) Raw waveform. (b) Waveform of differential data. (c) Extracted vehicle waveform.

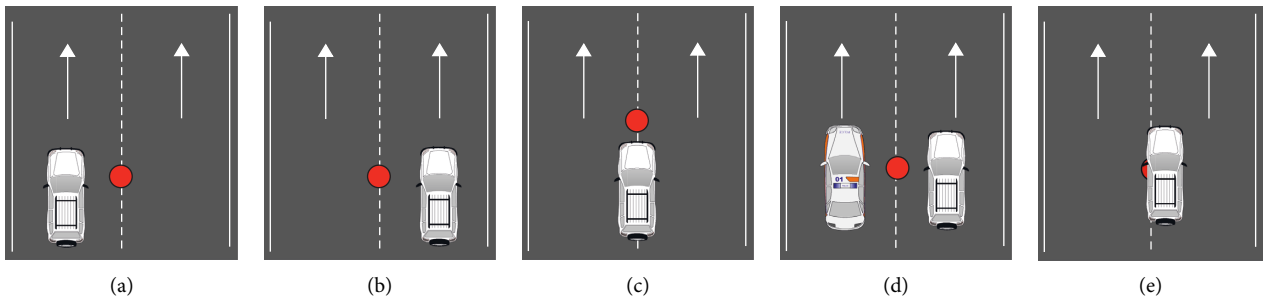

Figure 7: Schematic diagram of five detection scenarios. (a) Scenario 1. (b) Scenario 2. (c) Scenario 3. (d) Scenario 4. (e) Scenario 5.

which is called the cooperative working SRS system. According to the aforementioned characteristics, the result of a single SRS S_A can be classified into corresponding scenarios and recorded as (t_1,t_{p1},AL,AR), $(t_2,t_{p2},AL,AR)\ldots\ldots(t_n, t_{pn}, AL,AR)$, where t_i is the waveform start time and t_{pi} is the end time. AL represents vehicles passing on the left lane of the sensor S_A, while AR represents vehicles passing on the right lane. The value of AL, AR is 1 or 0, indicating whether vehicles are passing or not.

4. Vehicle Detection by Cooperative SRSs

A single SRS may mistakenly identify the vague working situations such as vehicles passing across lanes, oversized vehicles, or multiple vehicles passing in parallel. By utilizing multiple SRSs, the accuracy of distinguishing Scenarios 3, 4, and 5 can be greatly improved.

As shown in Figure 9, the SRSs are installed on the lane markings of the same road section. If a vehicle is detected by only one stud, it is impossible to identify the situations of two vehicles passing in parallel and a single vehicle passing over the studs, but the cooperative detection can distinguish these situations.

The left part of Figure 9 illustrates the vehicle driving scenarios, and the right part is the traffic flow information from the detection algorithm. The cases represented are summarized below.

(1) Case 1: a single vehicle passes on one lane. SRS detection results are $S_C(0,1)$ and $S_D(1,0)$, both of which indicate a vehicle passing on Lane 3, thereby improving the detection capability.

(2) Case 2: a vehicle passes over the lane line where the SRS S_B is located, and the detection result is $S_B(1,1)$. By combining the status of S_A and S_B, the identification of Scenario 3 can be improved.

(3) Case 3: one car on either side of S_C. The detection result is $S_B(0,1)$, $S_C(1,1)$, and $S_D(1,0)$. The three results improve the detection capability for Scenario 4.

(4) Case 4: this case shows a set of erroneous data detected by a single SRS. The erroneous detection result is $S_B(1,0)$ and $S_C(1,0)$. From S_A, S_B, and S_C test results, it can be inferred that the vehicle passed between S_B and S_C, calibrating the wrong result of S_B to $S_B(0,1)$.

Three SRSs are deployed for two-lane detection, by deploying the single-SRS detection algorithm, the results of which are S_x (t_1, t_{p1}, xL, xR), $(t_2, t_{p2}, xL, xR)\ldots\ldots(t_n, t_{pn}, xL, xR)$, $x = $ A, B, C. The calibration algorithm for vehicle detection based on Co-SRS is shown in Figure 10. The algorithm steps are presented below.

(1) Initialization: obtain the discrimination results $S_A(AL,AR)$, $S_B(BL,BR)$, $S_C(CL,CR)$, $a = AL + AR$, $b = BL + BR$, $c = CL + CR$.

(2) If a, b, $c > 0$, then two vehicles are side by side in adjacent lanes, and the result is corrected to $S_A(0,1)$, $S_B(1,1)$, $S_C(1,0)$.

(3) If $c = 0$; a, $b \neq 0$, then a vehicle passes between S_A and S_B, and the result is corrected to $S_A(0,1)$, $S_B(1,0)$.

(4) If $a = 0$; b, $c \neq 0$, then a vehicle passes between S_B and S_C, and the result is corrected to $S_B(0,1)$, $S_C(1,0)$.

(5) If a, $c = 0$; $b \neq 0$, then a vehicle passes over S_B, and the result is corrected to $S_B(1,1)$.

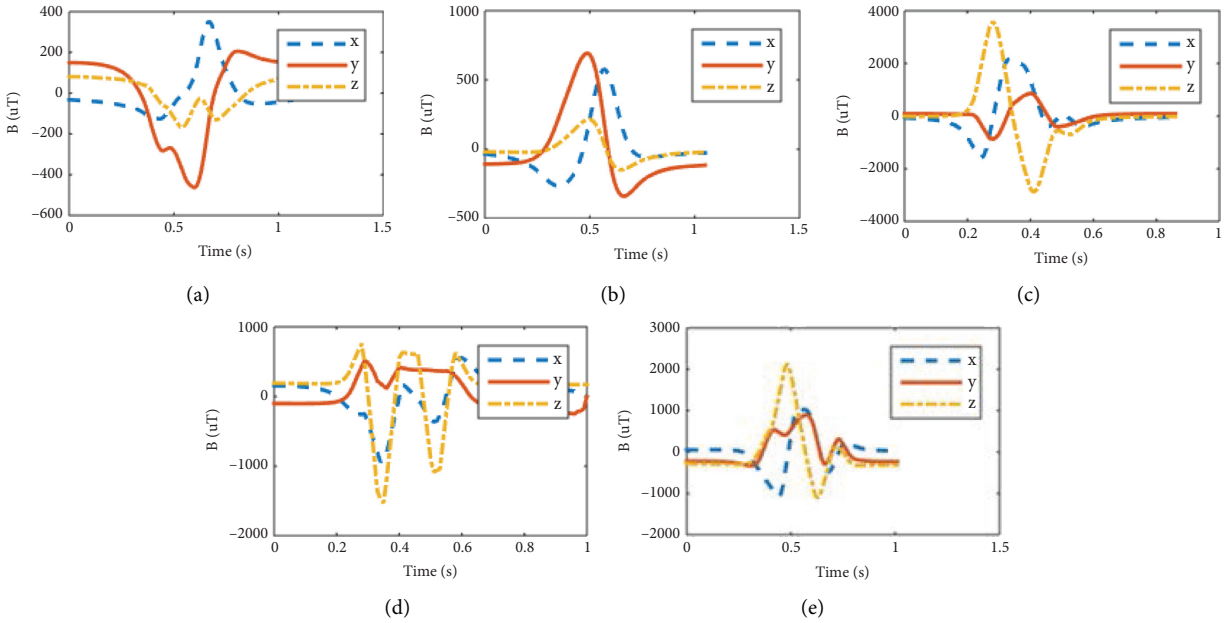

Figure 8: Waveform in different scenarios. (a) Scenario 1. (b) Scenario 2. (c) Scenario 3. (d) Scenario 4. (e) Scenario 5.

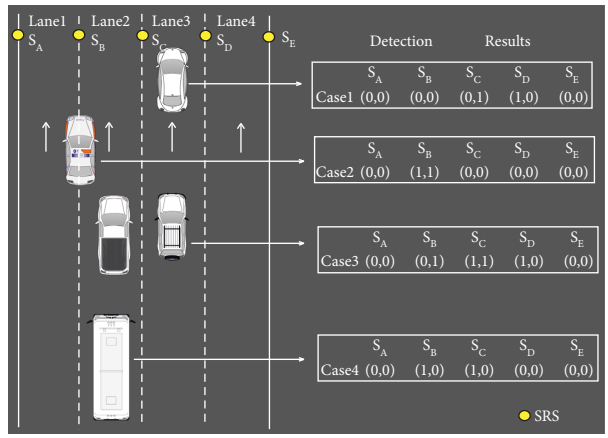

Figure 9: Diagram of cooperative SRS detection result calibration.

According to the calibrated $S_{A,B,C}$, $Num_{\text{lane1}} = [(\Sigma AR + \Sigma BL)/2]$ and $Num_{\text{lane2}} = [(\Sigma BR + \Sigma CL)/2]$. For multi-lane vehicle detection, $n+1$ SRSs are deployed on the section of n-lane road. Co-SRS calibration algorithm is deployed on tri-SRS repeatedly for multi-lane vehicle detection.

Collaborative SRS detection has the potential to improve the detection accuracy from two aspects. Firstly, the erroneous results of a single SRS can be cross validated and calibrated by cooperative SRSs. Secondly, it resolves the problems associated with a vehicle passing over/on the SRS and two vehicles in adjacent lanes side by side. Thirdly, Co-SRS can correct the misjudgment result caused by oversized vehicles driving in adjacent lanes.

5. Field Testing and Result Analysis

The experimental testing site was in an east-bound two-way 6-lane road named BinShui Road in Harbin, China. The geomagnetic inclination and declination are approximately 65° and 2°, respectively, as shown in Figure 11. The road studs were placed on the lane markings from east to west with a sampling frequency of 100 Hz each axis. The experiment was conducted on October 8, 2018, and the raw data were transmitted wirelessly to a remote computer station. Video surveillance signals were collected to count the actual numbers of vehicles on each lane.

5.1. Testing Results and Analysis of Single SRS Deployment. The actual traffic flow from video surveillance cameras is shown in Table 1. According to the driving direction, Lane 1, Lane 2, and Lane 3 are marked from road edge to centreline. Four SRSs as $S_{A,B,C,D}$ were installed on the lane lines of the one-way three-lane road from road edge to centreline correspondingly. Each SRS deploys the single-SRS vehicle detection algorithm for two-lane vehicle surveillance. Table 1 shows vehicle volumes of three lanes, respectively, detected

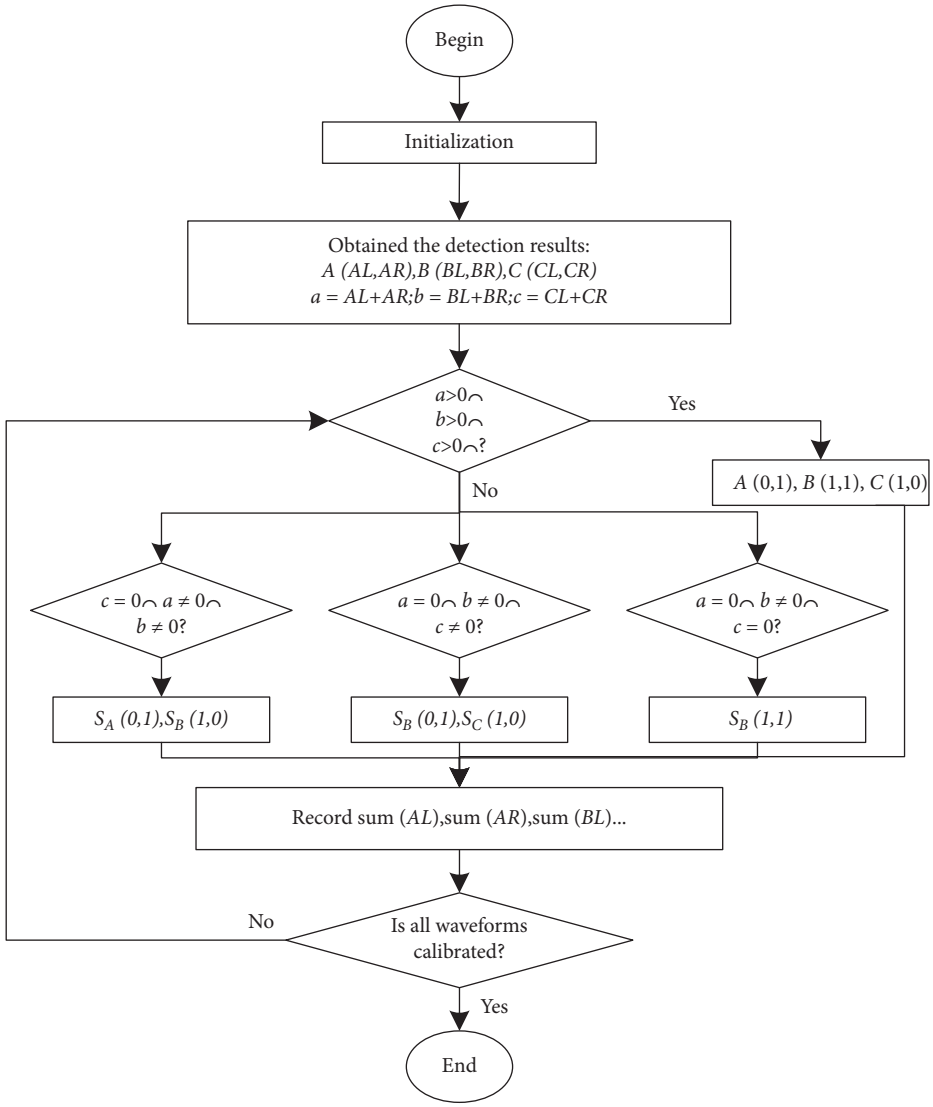

Figure 10: Co-SRS vehicle detection algorithm.

by S_B and S_c. The result of Lane 2 is the average value detection by S_B and S_c.

The lower correct detection rate is mainly attributed to the following reasons. (i) Scenario 3 is nonstandard driving behavior, in which the vehicle drives on the lane line instead of normal driving on the lane. In the single-SRS vehicle detection algorithm, the vehicles in Scenario 3 are simply split equally between Scenarios 1 and 2. (ii) If the wheel drive over the SRS or a vehicle changes from one lane to another, the test result may be misjudged as two vehicles passing in parallel as Scenario 4. (iii) Oversized vehicle driving in the adjacent lane causing huge magnetic field disturbance might affect the SRS detection results.

Normal driving should reduce the occurrence of Scenarios 3 and 5 and the error in Scenario 4, which should increase the correct detection rate in Lane 2. Furthermore, a higher detection accuracy should result from cross validation of the results from multiple SRSs deployed on each lane line of a road section.

5.2. Cooperative SRS Detection Results and Description. Four SRSs were installed on the lane lines of a one-way three-lane road. Co-SRS calibration algorithm was deployed repeatedly on (S_A, S_B, S_C) and (S_B, S_C, S_D) to complete the 3-lane discrimination results. Table 2 shows the multi-lane vehicle detection results achieved by Co-SRS calibration; the correct detection rate is about 98%. Compared with the detection results of a single SRS, the cooperative SRSs greatly increase the correct detection accuracy even in non-standard driving situations.

The experimental test results indicate the following:

(1) The general detection of vehicles does not consider the situation of vehicles crossing the lane markings. If the non-standard driving situation is removed, the accuracy of single SRS detection will be greatly improved.

(2) The cooperative SRSs can accurately distinguish the situations of vehicle passing over the detector and two vehicles passing in parallel.

Figure 11: The experiment of an east-west road in Harbin.

Table 1: Traffic volume detection by a single SRS.

	Traffic volume				
	0–15 min	15–30 min	30–45 min	45–60 min	Total
Lane 1	26	18	29	17	90
Lane 1 (true)	24	12	29	17	82
Accuracy	91.7%	50%	100%	100%	90.2%
Lane 2	81	90	88	89	351
Lane 2 (true)	83	95	92	91	361
Accuracy	97.6%	94.7%	95.7%	97.8%	97.2%
Lane 3	62	49	65	52	228
Lane 3 (true)	65	53	70	55	243
Accuracy	95.4%	92.5%	92.9%	94.6%	93.8%

Table 2: Traffic volume detection by cooperative SRSs.

	Traffic volume				
	0–15 min	15–30 min	30–45 min	45–60 min	Total
Lane 1	25	12	29	17	83
Lane 1 (true)	24	12	29	17	82
Accuracy	95.8%	100%	100%	100%	98.8%
Lane 2	82	95	88	89	354
Lane 2 (true)	83	95	92	91	361
Accuracy	98.8%	100	95.7%	97.8%	98.1%
Lane 3	64	52	68	55	238
Lane 3 (true)	65	53	70	55	243
Accuracy	98.5%	98.1%	97.1%	100	98.4%

6. Conclusion

The self-sustained SRSs installed on the lane markings can accurately detect traffic volume on multi-lane roads. The vehicle position can be identified by the classification feature. It can also distinguish the situation where vehicles pass in parallel. It eliminates the influence of vehicles on the adjacent lanes. The method is simple and highly efficient. Few samples are needed, and the detection accuracy can be up to 98%.

This research is superior in the following aspects:

(1) Most researchers detect traffic volume without considering any lane changing behavior. But the situation of vehicles crossing the lane markings is quite common and cannot be ignored. The proposed sensor network can also detect multi-lane traffic flow. It demonstrates high detection accuracy.

(2) Compared to traditional vehicle detection methods, the SRS installed on the lane line is able to provide safety assurance by light guidance with the same correct detection rate as middle-installed commercial intrusive sensor up to 98% correct detection rate.

(3) The SRS has the potential for large-scale deployment due to its low-cost, self-power supply, non-intrusive nature, and value-added services. The high level of automation enables the provision of various value-added services not available from current systems such as congestion recognition/warning, light driving guidance, safety-distance warning, and fog-zone warning. Other applications including parking management, smart zebra marking, and vehicle counting have been developed and demonstrated in the cities of Harbin, Shenzhen, and Ningbo in China. The collaborative detection of multiple SRSs has a promising application prospect in intelligent transportation fields.

Data Availability

The data used to support the findings of this study are available from the corresponding author upon request.

Conflicts of Interest

The authors declare that they have no conflicts of interest.

Acknowledgments

This research was supported by the National Natural Science Foundation of China (51578197 and 51578198).

References

[1] L. D. Vanajakshi, B. M. Williams, and L. R. Rilett, "Improved flow-based travel time estimation method from point detector data for freeways," *Journal of Transportation Engineering*, vol. 135, no. 1, pp. 26–36, 2009.

[2] S. Gontarz, P. Szulim, J. Seńko, and J. Dybała, "Use of magnetic monitoring of vehicles for proactive strategy development," *Transportation Research Part C: Emerging Technologies*, vol. 52, pp. 102–115, 2015.

[3] W. Liao, M. Liu, and Q. Meng, "Mixed traffic information collection system based on pressure sensor," *Physics Procedia*, vol. 25, pp. 726–732, 2012.

[4] Y. Wan, Y. Huang, and B. Buckles, "Camera calibration and vehicle tracking: highway traffic video analytics," *Transportation Research Part C: Emerging Technologies*, vol. 44, pp. 202–213, 2014.

[5] H. S. Fimbombaya, N. H. Mvungi, N. Y. Hamisi, and H. U. Iddi, "Enhanced magnetic wireless sensor network algorithm for traffic flow monitoring in low-speed congested traffic," *Journal of Electrical and Computer Engineering*, vol. 2020, no. 4, 8 pages, Article ID 5875398, 2020.

[6] V. Markevicius, D. Navikas, D. Miklusis et al., "Analysis of methods for long vehicles speed estimation using anisotropic magneto-resistive (AMR) sensors and reference piezoelectric sensor," *Sensors*, vol. 20, no. 12, 2020.

[7] Z. Zhao, Y. Chen, and W. Yi, "Design of wireless vehicle detector based on AMR sensor," *Electronic Measurement Technology*, vol. 36, no. 1, pp. 1–7, 2013.

[8] X. Zhang and H. Huang, "Vehicle classification based on feature selection with anisotropic magnetoresistive sensor," *IEEE Sensors Journal*, vol. 19, no. 21, pp. 9976–9982, 2019.

[9] P. Wang, J. Lai, Z. Huang, Q. Tan, and T. Lin, "Estimating Traffic Flow in Large Road Networks Based on Multi-Source Traffic Data," *IEEE Transactions on Intelligent Transportation Systems*, vol. 22, no. 99, pp. 1–12, 2020.

[10] J. Wang, G. Li, Y. Liu et al., "Vehicle Supervision System Based on MEMS Geomagnetic Sensor," in *Proceedings of the IEEE International Conference on Nano/Micro Engineered and Molecular Systems*, Shenzhen, China, January 2009.

[11] W. Tu, F. Xiao, L. Li, and L. Fu, "Estimating traffic flow states with smart phone sensor data," *Transportation Research Part C: Emerging Technologies*, vol. 126, no. 9, Article ID 103062, 2021.

[12] R. Nick, "Driver Behaviour in Response to Actively Illuminated Road Studs: A Simulator Study," Technical report PPR143, TRL, Bracknell, UK, 2006.

[13] A. Shahar and R. Br´emond, "Toward smart active road studs for lane delineation," in *Proceedings of the Transport Research Arena (TRA) 5th Conference: Transport Solutions from Research to Deployment*, Paris, France, April 2014.

[14] E. Sifuentes, O. Casas, and R. Pallas-Areny, "Wireless magnetic sensor node for vehicle detection with optical wake-up," *IEEE Sensors Journal*, vol. 11, no. 8, pp. 1669–1676, 2011.

[15] X. Bao, H. Li, D. Xu, L. Jia, B. Ran, and J. Rong, "Traffic vehicle counting in jam flow conditions using low-cost and energy-efficient wireless magnetic sensors," *Sensors*, vol. 16, no. 11, pp. 2–16, 2016.

[16] L. Meng, H. Wang, and W. Quan, "Vehicle detection using three-axis AMR sensors deployed along travel lane markings," *Journals & magazines. IET Intelligent Transport Systems*, vol. 11, no. 9, pp. 581–587, 2017.

[17] Z. Fang, Z. Zhao, and Y. Xuan, "A node design for intelligent traffic monitoring based on magnetic sensor," *Advances in Wireless Sensor Networks*, vol. 334, pp. 57–67, 2012.

[18] J. Chinrungrueng and S. Kaewkamnerd, *Wireless Magnetic Sensor Network for Collecting Vehicle Data*, Sensers, Christchurch, New Zealand, 2009.

[19] J. Chong, M. Zhao, and J. Li, "Noise reduction by magnetostatic coupling in geomagnetic-field sensors," *Journal of Magnetism and Magnetic Materials*, vol. 368, pp. 328–332, 2014.

[20] S. Taghvaeeyan and R. Rajamani, "Portable roadside sensors for vehicle counting, classification and speed measurement," *IEEE Transactions on Intelligent Transportation Systems*, vol. 15, no. 1, pp. 294–306, 2014.

[21] S. Cheung, S. Coleri, B. Dunda, G. Sumitra, C.-W. Tan, and P. Varaiya, "Traffic measurement and vehicle classification with a single magnetic sensor," *Transportation Research Record*, vol. 1917, no. 1, pp. 173–181, 2005.

[22] J. Lan, Y. Xiang, L. Wang, and Y. Shi, "Vehicle detection and classification by measuring and processing," *Measurement*, vol. 44, no. 11, pp. 174–180, 2011.

[23] W. Quan, H. Wang, and Z. Gai, "Spot vehicle speed detection method based on short-pitch dual-node geomagnetic detector - ScienceDirect," *Measurement*, vol. 158, Article ID 107661, 2020.